# On the anomalous generation of {001} loops during laser annealing of ion-implanted silicon

Luis A. Marqués[1,*], María Aboy[1], Iván Santos[1], Pedro López[1], Fuccio Cristiano[2], Antonino La Magna[3], Karim Huet[4], Toshiyuki Tabata[4], Lourdes Pelaz[1]

[1] *Departamento de Electricidad y Electrónica, Universidad de Valladolid, E.T.S.I. de Telecomunicación, 47011 Valladolid, SPAIN.*
[2] *LAAS-CNRS, Université de Toulouse, CNRS, 7 av. Du Col. Roche, 31031 Toulouse, FRANCE.*
[3] *CNR-IMM, VIII Strada 5, 95121 Catania, ITALY.*
[4] *SCREEN Semiconductor Solutions, Co., Ltd., LASSE, 14-30 rue Alexandre, 92230 Gennevilliers, FRANCE.*

**Abstract**

We combine focused experiments with molecular dynamics simulations to investigate in detail the formation of {001} loops in nanosecond laser-annealed silicon. We demonstrate that at temperatures close to the melting point, self-interstitial rich silicon is driven into dense liquid-like droplets that are highly mobile within the solid crystalline matrix. These liquid droplets grow by a coalescence mechanism and eventually transform into {001} loops through a liquid-to-solid phase transition in the nanosecond timescale.

Keywords: Si; Annealing; Atomistic simulation; Molecular dynamics; Extended defects.

## 1. Introduction

The process of self-interstitial clustering that follows ion-implantation in Si has attracted much attention over the last decades due to its technological relevance, especially for the fabrication of Si devices [1-3]. It is well known that ion implantation injects self-interstitials in the lattice that tend to cluster into extended defects following an Ostwald ripening mechanism [4]. Experiments show that the morphology of the generated extended defects depends on the particular implant and annealing conditions. At short anneals and low temperatures the most frequent are the so-called {113} defects, while for higher thermal budgets the dominant defects are {111} dislocations.

Recently, and for the first time, large {001} loops have been observed after ultra-fast laser annealing of ion-implanted Si samples [5]. However, some questions regarding their formation remain unanswered. Firstly, they formed in a time scale (few tens of nanoseconds) incompatible with the conventional Ostwald ripening mechanism [6]. Secondly, they were not expected from an energetic point of view, since the formation energy of {001} loops is higher than the corresponding to {111} dislocations. In the present paper we combine focused laser annealing experiments with molecular dynamics (MD), in order to get some insights into the physical mechanisms governing the formation of such "unconventional" {001} loops in Si.

## 2. Experimental results

First a bulk (001) Si wafer was implanted with 80 keV $Si^+$ to a dose of $2\times10^{14}$ ions/cm². These conditions ensure the formation of large interstitial-rich regions, while keeping the damage below the amorphization threshold. The implanted wafer was then laser annealed using a SCREEN-LASSE LT system based on pulsed UV irradiation ($\lambda = 308$ nm, pulse duration < 200 ns) with an energy density of 2.3 J/cm². Figure 1(a) shows a cross-section transmission electron microscopy (TEM) image of the sample. It is melted up to a depth of about 55 nm, and large

---

[*]Corresponding author. Tel.: +034-983185503; fax: +034-983423675. *E-mail address*: lmarques@ele.uva.es.

{001} loops are observed beyond. By means of phase-field simulations [7] we have calculated the maximum temperature profile in the sample, which is also displayed in Fig 1(a) superimposed to the TEM image. The variation of temperature with depth creates a thermal stress within the sample of around 1 GPa (see Fig. 1(c)).
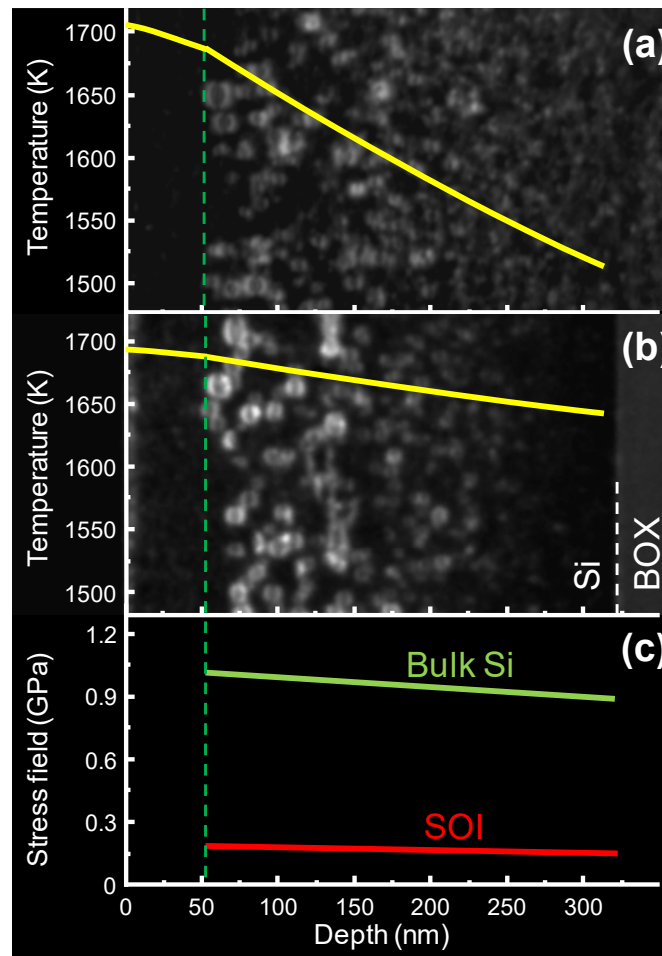


Fig. 1. Cross-section TEM micrographs from (a) the bulk Si substrate annealed at 2.3 J/cm$^2$, and (b) the SOI substrate annealed at 0.9 J/cm$^2$. Green dashed line indicates the melt depth. Superimposed are the corresponding local maximum temperature profiles calculated by phase-field simulations (yellow lines). Loops sizes in TEM image (b) are larger than those of image (a) at the same depth. (c) Maximum local stress field calculated with the thermo-elastic theory in the solid region below the maximum melt depth in bulk Si and SOI samples.

The impact of this thermal stress on the defect formation energy was initially proposed as a possible cause for the formation of {001} loops [5]. Indeed, for a bi-axial stress in the plane parallel to the surface, it is known that the modification of the defects formation energy value is proportional to the projection of the defect Burgers vector in the (001) plane and to the applied stress, while the formation energy of extrinsic type defects, such as those investigated in this work, increases (decreases) in the presence of a compressive (tensile) stress [8,9]. Formation energies of {001} and {111} dislocation loops were therefore calculated under different stress conditions and their values are shown in Fig. 2. For both dislocation types, the calculation is based on that of an edge dislocation [10] (in both cases the Burgers vector is perpendicular to the loop plane), while the stress field impact is calculated based on Refs. [8] and [9]. In the absence of external stress, the formation energy of {111} loops is lower than that of {001} loops, as expected (cf. solid curves in Fig. 2). The thermal stress created during the laser anneal has no impact on the formation energy of {001} loops (their Burgers vector is perpendicular to the stress plane). In contrast, the formation energy of {111} loops increases proportionally to the stress field. In the case of a 1 GPa external stress, their formation energy becomes higher than that of {001} loops (cf. dotted red curve in Fig. 2), therefore favoring the formation of {001} loops, in qualitative agreement with the observed results.
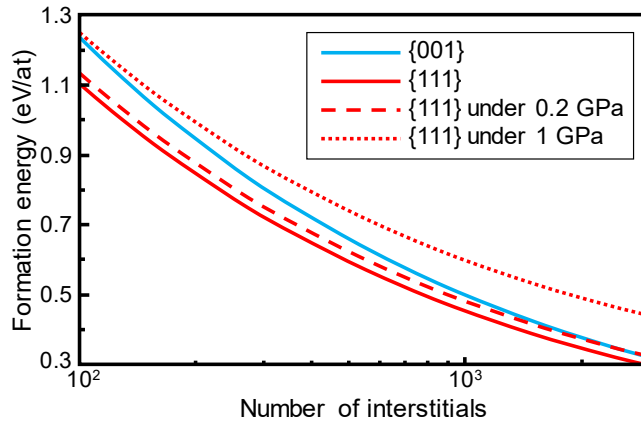
Fig. 2. Formation energy of {001} and {111} dislocation loops under different stress conditions.

We carried the same implantation experiment in a Silicon On Insulator (SOI) wafer. This sample was laser annealed at an energy density of 0.9 J/cm$^2$ to have the same melt depth than in the previous bulk Si case. Figure 1(b) shows the cross-section TEM image of the implanted and laser-annealed SOI sample, along with the maximum temperature profile estimated by means of phase-field simulations. The variation of temperature with depth is much smoother, which implies a local stress field of just around 0.2 GPa (see Fig. 1(c)). This stress value is not enough to invert the stability of {001} loops with respect to {111} dislocations, as shown in Fig. 2 (cf. dashed red curve). Still, the defects observed beyond the melt depth are of {001} type. Consequently, thermal induced stress alone cannot justify the presence of {001} loops. This fact, along with the inability of the Ostwald ripening mechanism to predict the formation of such large defects in just a few nanoseconds, indicate that new physical effects must be taking place during this process. Another interesting observation from these experiments is that {001} loop size appears to depend on temperature, as TEM images of Figs. 1(a) and 1(b) indicate.

## 3. Molecular dynamics simulations

We have designed specific MD simulations in order to understand the experimental observations and extract information regarding the formation of {001} loops at the atomic level. For the simulation setup, we have followed the same simulation scheme than in the preliminary work of Ref. [11]. We started from a perfect Si lattice in a cell of size 158 Å × 161 Å × 161 Å, containing 204624 atoms. Axis orientations were X [100], Y [011] and Z [0-11]. We used periodic boundary conditions to minimize finite size effects. We introduced 0.5% of excess interstitial atoms in tetrahedral positions chosen at random (a total of 1023 extra atoms). Generated samples were annealed at different temperatures to monitor how interstitial defects form and grow. To describe atom interactions we used the Tersoff 3 potential [12], which is known to give a good description of intrinsic defects, their aggregation process, and the liquid and amorphous phases of Si [13-15]. Unfortunately, this potential overestimates the Si melting point (2400 K instead of 1685 K [16]). However, this is not a serious drawback since it is possible to relate Tersoff temperatures $T_{Tersoff}$ with real ones $T_{Real}$ by using reduced temperatures $T^*$ obtained by the expression: $T^* = T_{Tersoff}/2400 = T_{Real}/1685$ ($T_{Tersoff}$ and $T_{Real}$ in Kelvin). This is a relatively simple approach usually employed in the MD community when using the Tersoff 3 potential, which allows to extract qualitative information from the simulations to be related to experimental data (however, calculated quantitative values should be taken with caution).

We have carried out annealing simulations of the initial sample with the excess interstitials at several values of $T^*$: 0.50, 0.70, 0.75, 0.80, 0.85 and 0.90, by using the open-source MD software package LAMMPS [17]. We have observed that at low annealing temperatures ($T^*$ from 0.50 to 0.75), initial single-interstitials and early formed di-interstitials diffuse very fast, giving rise to larger and immobile defects. This process continues until all mobile species are captured by large clusters. Subsequently, mobile species are emitted from immobile clusters and exchanged among them in a conventional Ostwald ripening mechanism [4]. This is consistent with the observation that effective diffusivities during the simulations show an initial plateau followed by a dependence close to 1/time

indicative of a halted diffusion (see Fig. 3). At the end of the simulations many different defects of small size are formed, most of them have less than 15 interstitials. Larger clusters are {111} rod-like defects, the precursors of {111} dislocation loops. A lot of (011) chains are also observed, which are the precursors of {113} defects. But most interstitials are in the form of tetra-interstitials in the Arai configuration [18], or small agglomerates of them (several snapshots taken during the annealing simulation at $T^* = 0.50$ can be observed in the Fig. 2 of Ref. [11]).

In the case of high annealing temperatures ($T^*$ from 0.80 to 0.90), the clustering process is completely different. Again single-interstitials and di-interstitials diffuse and interact forming larger defects. After 3 ns of annealing, apart from some Arai tetra-interstitials, large amorphous interstitial clusters are formed. They are highly mobile, as indicated by the second plateau in the curves of Fig. 3. Effective diffusivities ($\geq 10^{-5}$ cm$^2$/s) of these disordered interstitial clusters are lower but comparable to those corresponding to the highly-mobile species present at the early stages of the simulations. By calculating the pair distribution function of these amorphous agglomerates we have determined that they are in the liquid state and under compressive stress, which explains the high mobility they show in our simulations. Later these defects (liquid droplets) transform into large and immobile {001} loops. At the end of the simulations, some {111} dislocations are also observed, but most of the interstitials are in the form of {001} loops. Some isolated Arai tetra-interstitials are also present (several snapshots taken during the annealing simulation at $T^* = 0.80$ can be observed in the Fig. 4 of Ref. [11]). It is worth to note that this is the only interstitial defect with a regular atomic structure stable at these high temperatures, due to its high vibrational entropy [19].
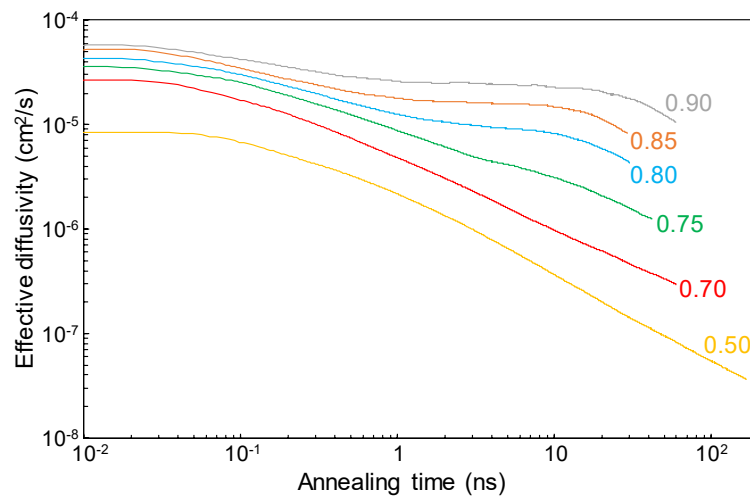


Fig. 3. Effective diffusivities as a function of time during annealing at several reduced temperatures. For low temperatures we see an initial plateau corresponding to the weighted average diffusivity of highly-mobile species followed by a dependence close to 1/time indicative of a halted diffusion when mobile interstitials defects become trapped in large immobile clusters. At higher temperatures an additional plateau at intermediate times is observed, revealing the onset of diffusion of the liquid interstitial clusters, which turn again into a dependence 1/time when they transform into immobile {001} loops.

Figure 4 shows the mean energy per atom within the interstitial clusters generated during all the annealing simulations as a function of their size. For the three lower temperatures, cluster energies decrease with size showing local minima at some "magic" numbers corresponding to very stable configurations. The minimum at size four corresponds precisely with the Arai tetra-interstitial, and sizes multiple of four with small agglomerates of such defect. Again, these results are consistent with a conventional Ostwald ripening process with dominance of stable ordered structures [4,20]. However, for reduced temperatures of 0.80 and above, the energy curves show only a local minimum for interstitial clusters of size four (the Arai tetra-interstitial as the only defect able to withstand such high temperatures), and then wide plateaus with a quasi-continuous energy distribution. These plateaus represent the liquid droplets, which dominate at high temperatures with respect to ordered structures due to their high configurational entropy. When they reach a certain size, they spontaneously transform into ordered planar {001} loops. The transformation (indicated by the sharp drops in the curves of Fig. 4) occurs at cluster sizes that increase with annealing temperature, which explains why higher temperatures produce larger {001} loops.
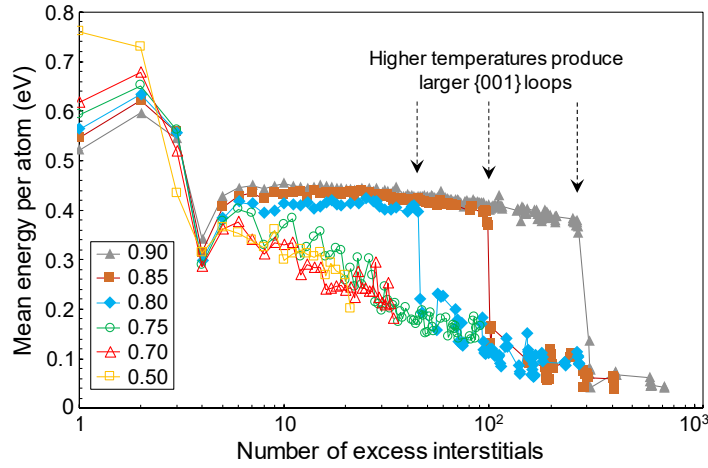
Fig. 4. Dependence of the interstitial cluster mean energy per atom with size at different annealing temperatures.

Liquid droplets adopt a quasi-spherical shape to minimize the surface-to-volume ratio and consequently the defect interfacial energy. We have observed that when two liquid interstitial aggregates moving through the Si lattice interact, first a "neck" connecting both pockets is generated, and then fast atomic redistribution leads to the recovery of the spherical shape in the final droplet (see Fig. 5). This kind of process, known as *coalescence*, is common for defect coarsening in metals [21-23]. However, our work appears to be the first evidence of such a mechanism for interstitial defect growth in Si. It is interesting to note that, when coalescence is completed and a new larger sphere is formed, the total number of atoms displaced from perfect lattice positions in the resulting droplet is larger than the sum of displaced atoms in the former defects. This means that liquid aggregates tend to occupy a larger volume per interstitial atom as they grow, which leads to a pressure release within the droplets, as it can be seen in Fig. 6 [24]. Again sharp drops indicate the transformation of liquid interstitial clusters into {001} loops. It is worth to note that defect pressures for the structural transformation decrease with annealing temperature. We have also plotted in Fig. 6 these pressure values as a function of $T^*$ along with the solid-liquid equilibrium line in the Si phase diagram [25]. At the early stages of the annealing simulations, generated interstitial clusters are small and the corresponding points in the diagram are above the solid-liquid line. As these liquid interstitial clusters coalesce and grow, their associated pressure decreases until they cross the solid-liquid equilibrium line. Then liquid droplets become undercooled, and after some incubation period they transform into regular {001} loops. The clear correlation between temperature and pressure values with the solid-liquid equilibrium line in the Si phase diagram indicates that the transformation of liquid droplets into {001} loops is, in fact, a first order phase transition. We have observed that the transformation starts with the nucleation of Arai tetra interstitials at the liquid droplet edges during the incubation period [11]. As previously mentioned, this is the only defect that can withstand temperatures close to the Si melting point. Once nucleated, Arai tetra-interstitials act as a template that promote the fast liquid droplet crystallization. Interstitial atoms in the final loop organize on {001} planes precisely because extra atoms in the Arai configuration are lying on such planes [18].
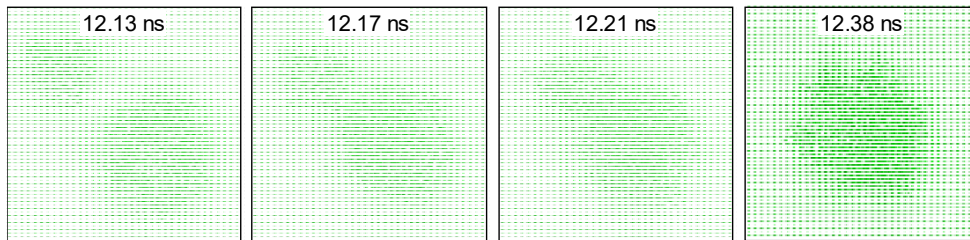


Fig. 5. ZY snapshots showing the coalescence of two interstitial droplets during annealing at $T^* = 0.90$. Times are measured from the start of the MD simulation. The number of atoms displaced from perfect lattice positions in the final droplet is 1527, larger than the sum of atoms displaced in the former clusters, 241 and 1135, respectively.
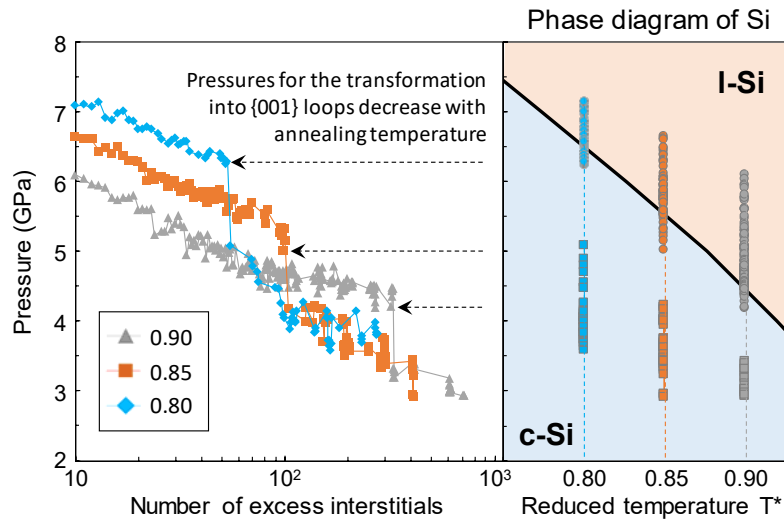
Fig. 6. Left graph: dependence with size of the interstitial cluster hydrostatic pressure at the three higher annealing temperatures. Right graph: pressure values represented as a function of $T^*$ along with the solid-liquid equilibrium line of the Si phase diagram [25]. Circles correspond to liquid interstitial clusters and squares to {001} loops.

## 4. Conclusions

We have performed dedicated self-implantation and laser annealing experiments in bulk and SOI Si samples in order to study the formation of extended defects under high-temperature and short-time anneal conditions. Experiments show the formation of large {001} loops instead of the conventional {111} dislocations. This observation is anomalous since {001} loops form within just a few nanoseconds, which is incompatible with the conventional Ostwald ripening mechanism, and in the absence of thermal-induced stress, which would justify the inversion of stability between {111} and {001} defects. We have used MD simulation techniques to investigate the physical mechanisms underlying the formation of the unconventional {001} loops. We have found that at annealing temperatures close to the melting point ($T^* \geq 0.80$), interstitial defect clusters: (a) are of liquid nature and highly mobile, (b) grow by means of a coalescence mechanism, and (c) transform into {001} loops when they reach a critical size depending on temperature. Simulations show that the transformation of liquid clusters into {001} loops is a first-order phase transition, and it occurs in the nanosecond time-scale from the spontaneous nucleation of Arai tetra-interstitials. MD simulation results explain and justify all the experimental observations on the formation of {001} loops in Si.

## Acknowledgements

## References

1. K. S. Jones, S. Prussin, and E. R. Weber, Appl. Phys. A 45, 1 (1988).
2. S. Takeda, Micros. Res. Techniq. 40, 313 (1998).
3. The International Technology Roadmap for Semiconductors, http://www.itrs.net/.
4. A. Claverie, B. Colombeau, B. D. Mauduit, C. Bonafos, X. Hebras, G. B. Assayag, and F. Cristiano, Appl. Phys. A 76, 1025 (2003).
5. Y. Qiu, F. Cristiano, K. Huet, F. Mazzamuto, G. Fisicaro, A. La Magna, M. Quillec, N. Cherkashin, H. Wang, S. Duguay, and D. C. Blavette, Nano Lett. 14, 1762 (2014).

6. We have run Kinetic Monte Carlo simulations with models based on Ostwald ripening for interstitial defect aggregation using the energetics reported in Fig. 2 under 1 GPa strain. In this case, {001} loops are favored versus other kind of extended defects, but simulations fail to predict the formation of large {001} loops in a timescale of just several nanoseconds, as they are observed in the experiments. Due to the slow exchange of mobile species among stable clusters associated to Ostwald ripening, defects are in the early stages of ripening at this time scale, instead of in a mature state corresponding to the sizes observed experimentally.

7. K. Huet, G. Fisicaro, K. Venturini, H. Besaucele, and A. La Magna, Appl. Phys. Lett. 95, 231901 (2009).

8. A. J. Pitera and E. A. Fitzgerald, J. Appl. Phys. 97, 104511 (2005).

9. M. Nastasi, T. Höchbauer, J.-K. Lee, A. Misra, J. P. Hirth, M. Ridgway, and T. Lafford, Appl. Phys. Lett. 86, 154102 (2005).

10. D. Hull and D. J. Bacon, in 'Introduction to Dislocations', Elsevier (2011).

11. L. A. Marqués, M. Aboy, M. Ruiz, I. Santos, P. López, and L. Pelaz, Mat. Sci. Semicond. Process. 42, 235 (2016).

12. J. Tersoff, Phys. Rev. B 38 (1988) 9902.

13. M. Ishimaru, S. Munetoh, and T. Motooka, Phys. Rev. B 56, 15133 (1997).

14. S. S. Kapur and T. Sinno, Phys. Rev. B 82, 045205 (2010).

15. K. J. Dudeck, L. A. Marqués, A. P. Knights, R. M. Gwilliam, and G. A. Botton, Phys. Rev. Lett. 110, 166102 (2013).

16. L. A. Marqués, L. Pelaz, M. Aboy, and J. Barbolla, Nucl. Instrum. Methods Phys. Res. B 216, 57 (2004).

17. S. Plimpton, J. Comp. Phys. 117, 1 (1995).

18. N. Arai, S. Takeda, and M. Kohyama, Phys. Rev. Lett. 78, 4265 (1997).

19. S. S. Kapur and T. Sinno, Appl. Phys. Lett. 93, 221911 (2008).

20. N. E. B. Cowern, G. Mannino, P. A. Stolk, F. Roozeboom, H. G. A. Huizing, J. G. M. van Berkum, F. Cristiano, A. Claverie, and M. Jaraíz, Phys. Rev. Lett. 82, 4460 (1999).

21. R. S. Barnes and D. J. Mazey, P. Roy. Soc. A-Math. Phy. 275, 47 (1963).

22. A. Weck, D. S. Wilkinson, E. Maire, and H. Toda, Acta Mater. 56, 2919 (2008).

23. T. D. Swinburne, K. Arakawa, H. Mori, H. Yasuda, M. Isshiki, K. Mimura, M. Uchikoshi, and S. L. Dudarev, Sci. Rep. 6, 30596 (2016).

24. Atomic hydrostatic pressure values are computed using the stress/atom command in LAMMPS. Then we add the atomic values for all the atoms belonging to the defect cluster to get the total cluster pressure as represented in Fig. 6. Values are averaged for each defect cluster size.

25. C. C. Yang, J. C. Li, and Q. Jiang, Solid State Commun. 129, 437 (2004).